3D TIME MIGRATION VELOCITY MODEL BUILDING USING CRS-BASED PRESTACK DIFFRACTION SEPARATION

P. Bakhtiari Rad, Y. Xie, C. Vanelle, and D. Gajewski

email: *parsa.bakhtiari.rad@studium.uni-hamburg.de*

keywords: *3D diffraction separation, prestack data enhancement, migration velocity model building*

ABSTRACT

Time migration still serves as the first reliable tool for seismic imaging. It is fast and robust especially in the case of voluminous 3D data sets. However, time migration velocity determination in areas with steep dips faces challenges and requires several updates of stacking velocities in order to remove the effect of reflector dip. In this paper, we propose a data-driven approach based on the common-reflection-surface (CRS) method to build a time migration velocity model purely tuned to diffractions. We use a prestack diffraction separation technique to generate diffraction gathers. Application to a complex 3D data set confirms the potential for diffraction separation as well as for time migration velocity model building using diffractions.

INTRODUCTION

For decades time migration has been widely used by the industry for imaging since it delivers a first reliable image of the sub-surface and it is fast and robust. Moreover, it is not very sensitive to velocity errors. For horizontally-layered media, the stacking velocities are RMS velocities and coincide with the time migration velocities, whereas in complex media, stacking velocities deviate from the migration velocities and thus lead to imaging problem, e.g., non-flat common image gathers (CIG). To solve the problem, time-migration velocities are updated in an iterative fashion based on residual move-out analysis of reflected events (e.g., Robein, 2003). As a result, reflections can be aligned horizontally in the CIG's. However, if diffraction-only data are available, the resulting stacking velocities are dip-independent and thus do not need updates to remove the effect of the dip. Therefore, in the case of diffraction data, stacking velocities can immediately be used as time migration velocities.

In order to obtain diffraction-only data, a multitude of methods exist for the separation of diffracted from reflected events (see, e.g. Khaidukov et al., 2004; Fomel et al., 2006; Moser and Howard, 2008; Dell and Gajewski, 2012). In general, diffraction separation in the prestack domain has higher potential than in the poststack domain since the prestack method can be combined with the data enhancement facility of the partial CRS stack technique introduced by Baykulov and Gajewski (2009). In this work, we therefore extend the prestack diffraction separation workflow to generate 3D diffraction-only data.

After introducing the method, we evaluate its performance for a 3D complex synthetic data set. First, we compare the separation potentials of the workflow in the pre- and poststack domain. In a second step, we determine migration velocities from the so-obtained diffraction-only data and perform a time-migration.

3D COMMON-REFLECTION-SURFACE

The CRS stacking operator for the zero-offset (ZO) simulation is given by (see, e.g. Schleicher et al., 1993; Müller, 2003) as

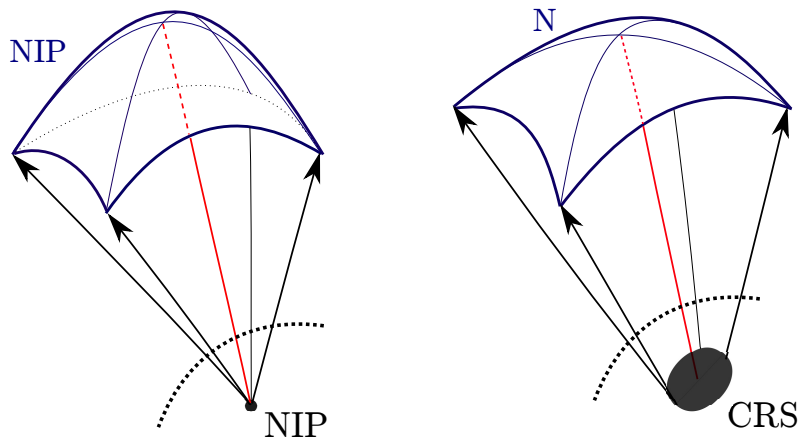

Figure 1: The meaning of the ZO CRS wavefield attributes: (left) curvature of the so-called normal-incident-point (NIP) wavefront which is emitted from a fictitious point source on reflector and, (right) curvature of the normal wavefront, which is emitted from a curved reflector element, the so-called common-reflection-surface. Both curvatures are measured at the surface.

$$t^2_{CRS}(\Delta\mathbf{x}_m, \mathbf{h}) = (t_0 + 2\mathbf{p}\Delta\mathbf{x}_m)^2 + 2t_0\left(\Delta\mathbf{x}_m^{\mathbf{T}}\mathbf{M}_N\Delta\mathbf{x}_m + \mathbf{h}^{\mathbf{T}}\mathbf{M}_{NIP}\mathbf{h}\right), \tag{1}$$

where $\mathbf{M}_N$ and $\mathbf{M}_{NIP}$ are symmetric 2×2 matrices that describe the curvatures of the normal and normal-incident-point (NIP) wavefronts, respectively (Hubral, 1983). These two principle curvatures have physical meaning. They are obtained by two artificial seismic experiments. The NIP wave is emitted from a fictitious point source on the reflector and the normal wave is emitted from a curved reflector element, the common-reflection-surface (see Figure 1). Vector $\mathbf{p}$ is the slowness vector that contains the dip angle and azimuth of the central ray (the red line in Figure 1). Furthermore, $\Delta\mathbf{x}_m$ is the midpoint displacement vector with respect to the central ray coordinate, and $\mathbf{h}$ is the half-offset vector. The 3D CRS stacking method has thus eight independent attributes, which are determined by means of coherency analysis (e.g., Müller, 2003).

CRS for diffractions

According to the CRS theory, a diffractor is associated with a reflector of infinite curvature and indefinite orientation (Mann, 2002). Consequently, for a diffracted event from a point diffractor, the matrices $\mathbf{M}_N$ and $\mathbf{M}_{NIP}$ for the curvature become identical, implying component-wise equality of $\mathbf{M}_{NIP}$ and $\mathbf{M}_N$. In this case, equation (1) can be simplified to

$$\begin{aligned} t^2_D(\Delta\mathbf{x}_m, \mathbf{h}) &= (t_0 + 2\mathbf{p}\Delta\mathbf{x}_m)^2 + 2\,t_0\left(\Delta\mathbf{x}_m^{\mathbf{T}}\mathbf{M}_{NIP}\Delta\mathbf{x}_m + \mathbf{h}^{\mathbf{T}}\mathbf{M}_{NIP}\mathbf{h}\right) \\ &= (t_0 + 2\mathbf{p}\Delta\mathbf{x}_m)^2 + 2\,t_0\left(\Delta\mathbf{x}_m + \mathbf{h}\right)^{\mathbf{T}}\mathbf{M}_{NIP}\left(\Delta\mathbf{x}_m + \mathbf{h}\right) \quad . \end{aligned}$$

This equation represents the 3D CRS-based diffraction stacking operator.

As already mentioned for a point scatterer, the equality of the curvature matrices allows to identify the diffracted events and separate them from reflected energy. However, because of noise and the band-limited nature of seismic data, the equality, which is the kernel of diffraction imaging, is not exactly fulfilled in practice. Therefore, we apply a weighting function as a filter for diffraction separation. In this study, we extend the 2D diffraction filter proposed by Dell and Gajewski (2011) to three dimensions, i.e.,

$$W_D = \exp\left\{-\sum_{i=0}^{1}\sum_{j=0}^{1}\left|\frac{M_N^{ij} - M_{NIP}^{ij}}{M_N^{ij} + M_{NIP}^{ij}}\right|\right\}, \tag{2}$$

where M_N^{ij} and M_{NIP}^{ij} are the components of the corresponding matrices. If these components are close to each other, i.e., for diffractions, the function W_D will be close to one. The function value will be close to zero for reflections. Therefore, a user-chosen threshold can be applied to identify diffractions: If the value of W_D is above the threshold, the data are stacked and if it is below the threshold, the data are not stacked. The choice of the threshold depends on the complexity of the subsurface. If the threshold is chosen too low, reflection events are not fully suppressed. On the other hand, a too high choice of the threshold suppresses diffracted energy as well. The best suitable threshold thus depends on the complexity of the medium and the data quality in general (Dell and Gajewski, 2011).

CRS-BASED WORKFLOW FOR TIME IMAGING

In order to combine the features of diffraction processing with the CRS method, we suggest the following strategy to obtain time-migration velocities tuned to diffraction-only data:

1. Determination of the 3D CRS wavefield attributes.
2. Evaluation of the separation criterion with proper choice of the separation threshold based on the complexity of the subsurface.
3. Finding the according ZO time and CRS attributes for each offset sample using a 3D extension of the solution suggested by Baykulov and Gajewski (2009).
4. Execution of a partial CRS stack (Baykulov and Gajewski, 2009) in 3D for diffractions with an optimal aperture in both $\mathbf{h}$ and $\Delta\mathbf{x}_m$ directions to generate diffraction-only gathers.
5. Automatic time migration velocity analysis (MVA) for each diffraction gather based on the semblance norm (Taner and Koehler, 1969).
6. Prestack time migration using velocities determined from diffraction-only data.

In the following section, we demonstrate the potential of the proposed workflow for time-imaging by application to a 3D complex data set.

APPLICATION: SEG/EAGE SALT MODEL

In order to evaluate the performance of the workflow, we chose the SEG/EAGE wide azimuth (WAZ) complex data set. The data set consists of 26 sail-lines separated by 320 m, 96 shots per line with 80 m shot interval, 8 cables per shot, 68 receivers per cable, and a 40 m receiver interval. The model describes a complex salt body in the Gulf of Mexico. The top of the salt is rugged and generates different patterns of diffraction events. We chose a portion of the data over the salt body for processing with in-line ranges from 94 to 286 and cross-line ranges from 43 to 428. The common-data-point (CDP) bin size was 40 $\times$ 20 m^2 in in- and cross-line (or x-line) directions, leading to a maximum fold of 18. The offset ranges from 0 to 2680 m. Figure 2 displays the model.

The CRS stacking method was applied to the data, where we used the pragmatic approach (Müller, 2003) to obtain the wavefield attributes. Subsequently, post- and prestack diffraction separation were performed. Figure 3(a) shows the stacked section of in-line 200 from the center of the salt body prior to diffraction separation. It exhibits different diffraction patterns, as expected, as well as conflicting dips, where diffractions and reflections intersect. Figures 3(b) and 3(c), respectively, display ZO diffraction-only data as a result of post- and prestack diffraction separation. We used the same threshold of 0.85 for both cases. By comparison, it is evident that the prestack diffraction separation leads to a better result than the poststack diffraction separation: Not only are the diffracted events considerably better separated but the data quality was also enhanced. However, some residual reflection energy is still present in both sections. Figures 4(a) to 4(c) show according results for x-line 300. Again, the prestack diffraction separation exhibits higher potential regarding diffraction separation and data enhancement compared to the poststack method.

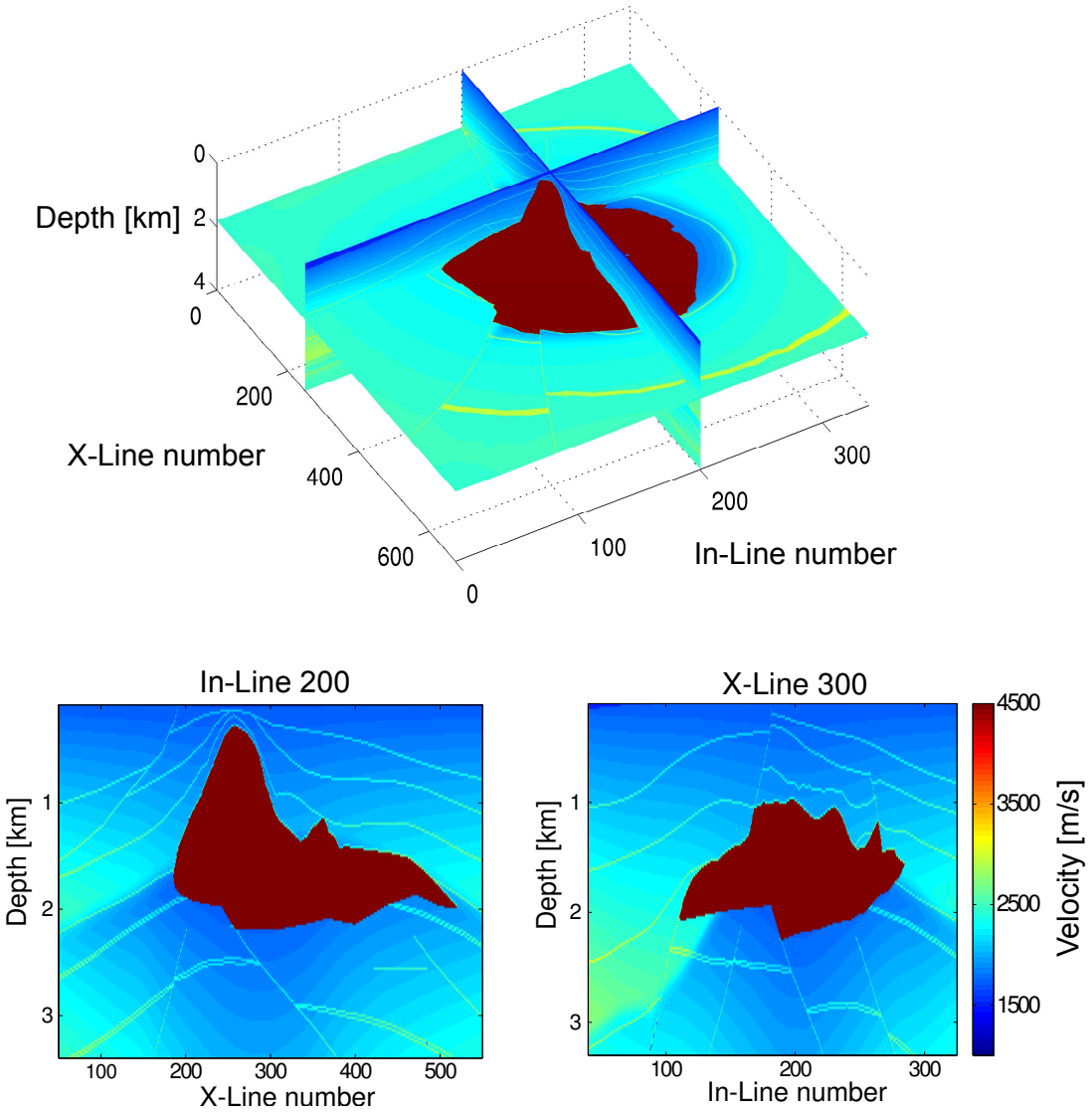

Figure 2: The SEG/EAGE C3 WA salt model. The velocity varies from 1500 to 4500 m/s. The model describes a salt body in the Gulf of Mexico. The rugged top-of-the-salt generates different diffraction patterns.

For further evaluation, we have chosen a time slice through the center of the data set at about 2.5 s. Figures 5(a) to 5(c) display the stacked section and the post- and pre-stacked diffraction-only data, respectively. Although most of the diffracted energy is separated well, some residual reflections are still present in the data. Furthermore, some gaps and terminations are present in both sections since conflicting dips are not yet handled in the workflow and thus lead to difficulties in such regions.

Finally, we have determined time migration velocities from the diffraction-only data obtained in the previous step. Figure 6 displays a common data point gather from in-line 130 and the corresponding velocity spectra before and after prestack diffraction separation, respectively. By comparing the results, we could confirm that indeed mostly diffractions are present in the diffraction-only data and only few residuals of reflections remain. We conclude that prestack diffraction separation leads to higher coherency and better focused picks for time migration velocity analysis. Figure 7 displays corresponding results for x-line 300. Again, the prestack diffraction separation leads to higher coherency and better focused picks.

Figure 8 displays prestack time migration results before and after prestack diffraction separation for in-line 130, Figure 9 for x-line 300 and Figure 10 for a time slice at 2.5 s. We observe that the top-of-the-salt is imaged well and the diffractions are generally better collapsed after prestack diffraction separation, as outlined by the red arrows in the figure, suggesting that diffraction velocities can be a good supplement in regions where migration velocities are otherwise hard to obtain. However, diffraction-based imaging may fail and lead to blurred images in regions without enough diffractions. Conflicting dips and unfocused diffractions due to more complex diffractor geometry than the point-type considered in this work may also deteriorate diffraction velocity model building and subsequent imaging.

CONCLUSIONS AND OUTLOOK

We proposed a 3D data-driven CRS-based workflow for time-imaging tuned to diffraction velocities. It is based on a 3D extension of the prestack diffraction separation and combines a diffraction weighting function with the partial CRS stack technique to generate diffraction gathers. In addition to comparing the prestack diffraction separation with poststack diffraction separation on a 3D complex synthetic data set, time-migration was carried out using diffraction velocities. The results confirm that diffraction separation in the pre-stack domain is superior to the post-stack diffraction separation. Furthermore, we find that time migration velocity model building based on diffraction-only data has indeed a high potential. However, some issues remain that need to be resolved in order to exploit the full potential of the method. Examples for such issues are conflicting dips and diffractor geometries that differ from the so-far considered point diffractors, e.g., edge and tip diffractions. Both topics are currently under investigation in the Applied Seismics Group Hamburg.

ACKNOWLEDGEMENTS

We thank the members of the Applied Seismics Group Hamburg for continuous discussions. The synthetic seismic data were produced by the Sandia National Laboratories (SNL). This work was partially supported by the sponsors of the WIT consortium.

REFERENCES

Baykulov, M. and Gajewski, D. (2009). Prestack seismic data enhancement with partial common-reflection-surface (CRS) stack. *Geophysics*, 74:V49–V58.

Dell, S. and Gajewski, D. (2011). 3D CRS-attributes based diffraction imaging. *73rd Conference and Technical Exhibition, EAGE, Extended Abstracts*, page B019.

Dell, S. and Gajewski, D. (2012). 3D velocity model building based on diffractions. *5th EAGE St. Petersburg International Conference and Exhibition on Geosciences, Extended Abstracts*.

Fomel, S., Landa, E., and Taner, M. T. (2006). Poststack velocity analysis by separation and imaging of seismic diffractions. *Geophysics*, 72:U89–U94.

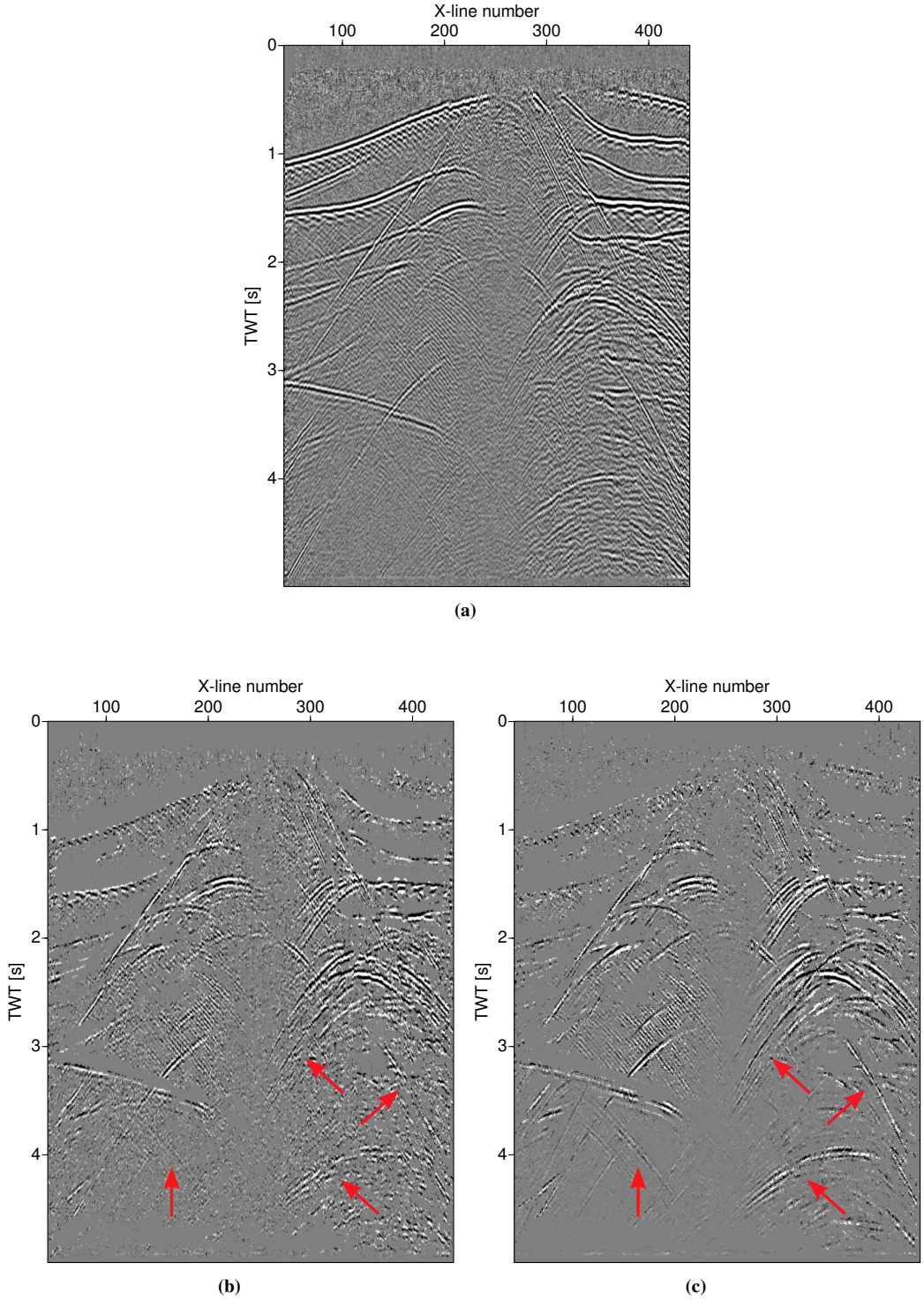

Figure 3: Results for in-line 200: (a) stacked section prior to diffraction separation, (b) ZO diffraction-only data after poststack diffraction separation, (c) ZO diffraction-only data after prestack diffraction separation. Red arrows indicate events that were better focused after prestack diffraction separation.

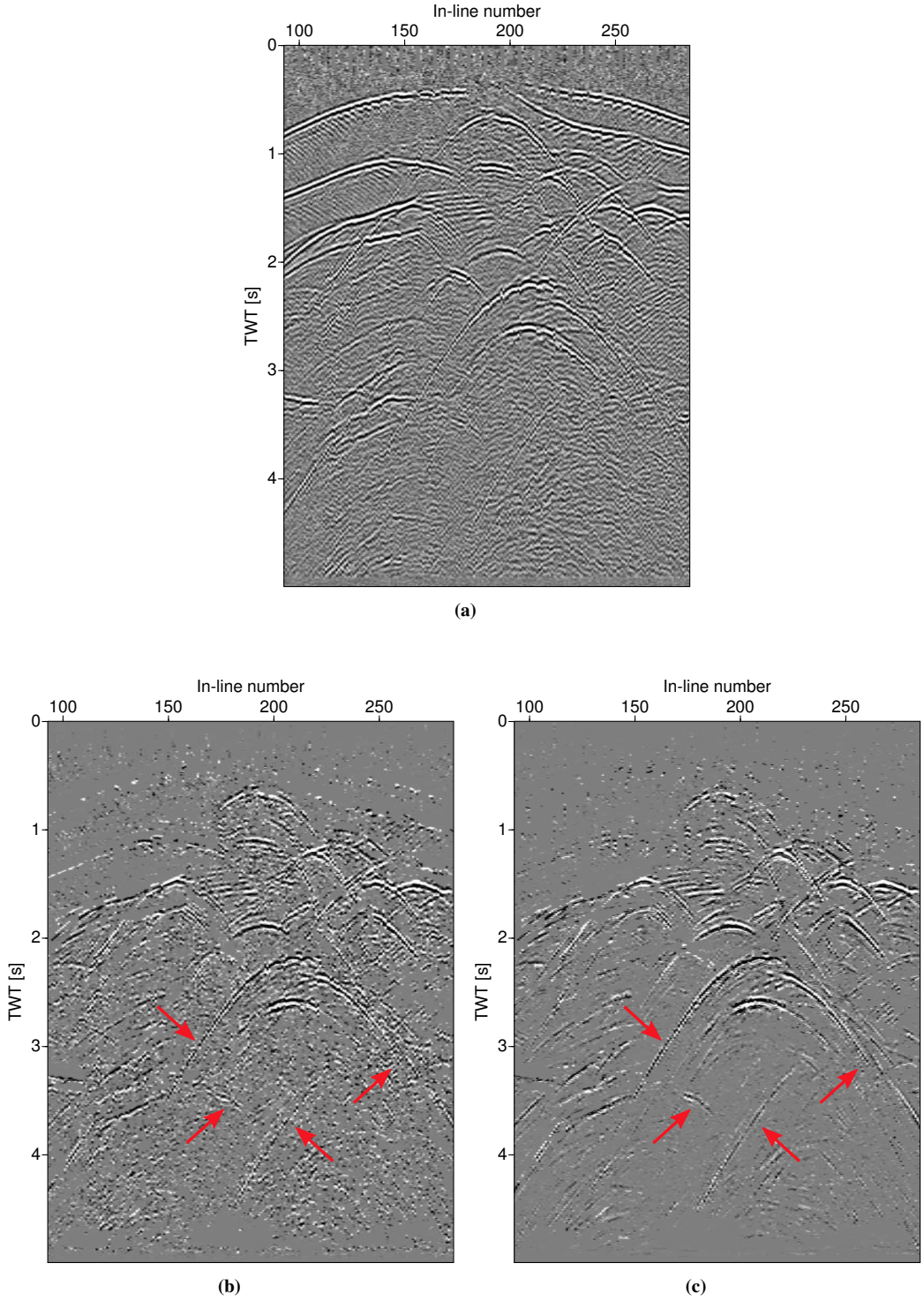

Figure 4: Results for x-line 300: (a) stacked section prior to diffraction separation, (b) ZO diffraction-only data after poststack diffraction separation, (c) ZO diffraction-only data after prestack diffraction separation. Red arrows indicate events that were better focused after prestack diffraction separation.

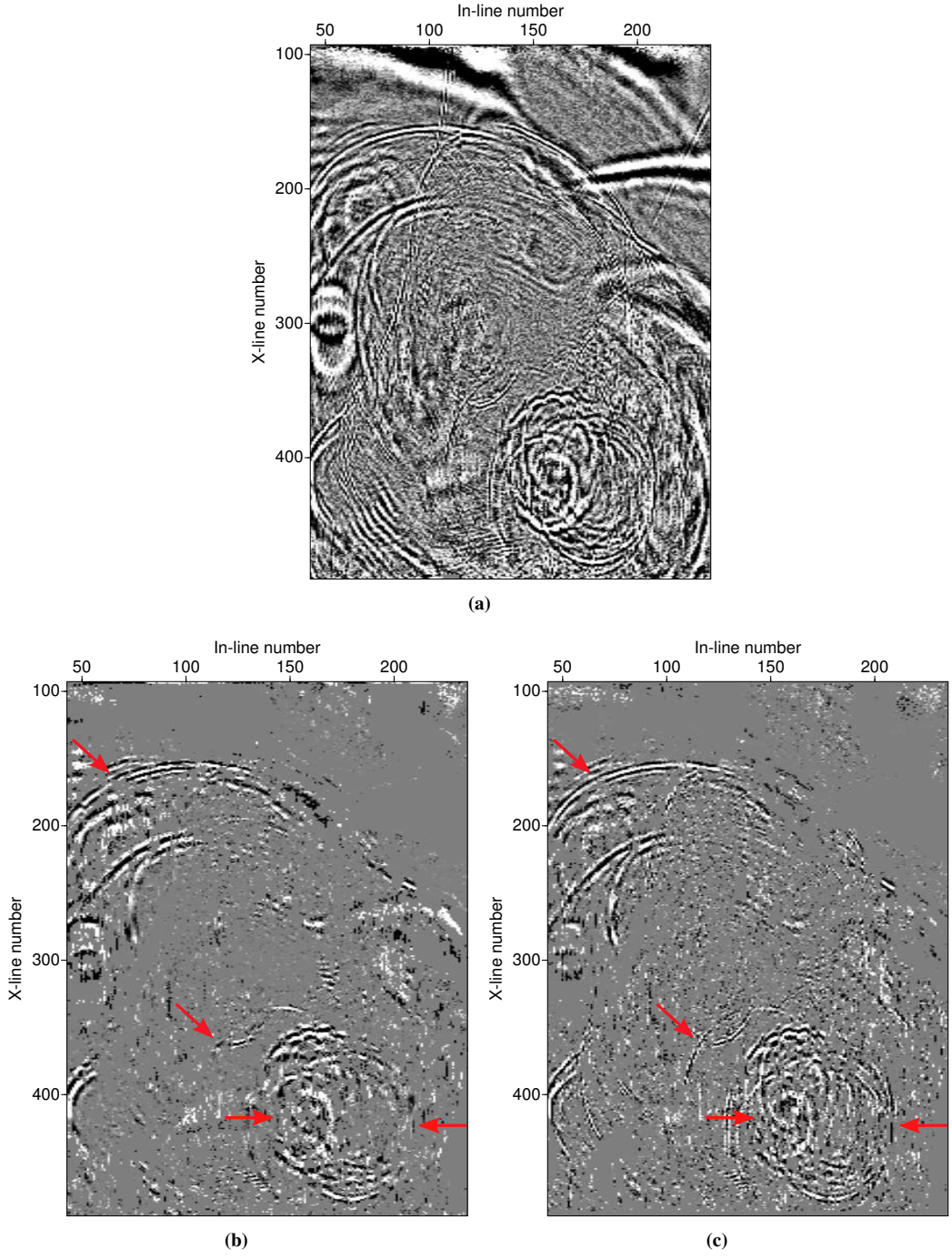

Figure 5: Results for time slice at 2.5 s: (a) stacked section prior diffraction separation, (b) ZO diffraction-only data after poststack diffraction separation, (c) ZO diffraction-only data after prestack diffraction separation. Red arrows indicate events that were better focused after prestack diffraction separation.

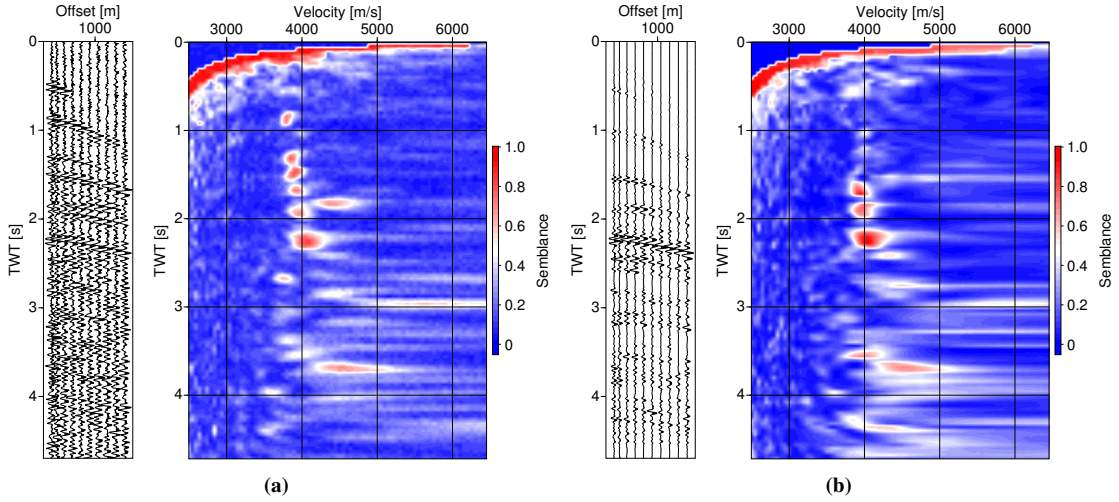

Figure 6: Results for a common-data-point (CDP) gather from in-line 130 and the corresponding velocity spectrum (a) before and (b) after prestack diffraction separation.

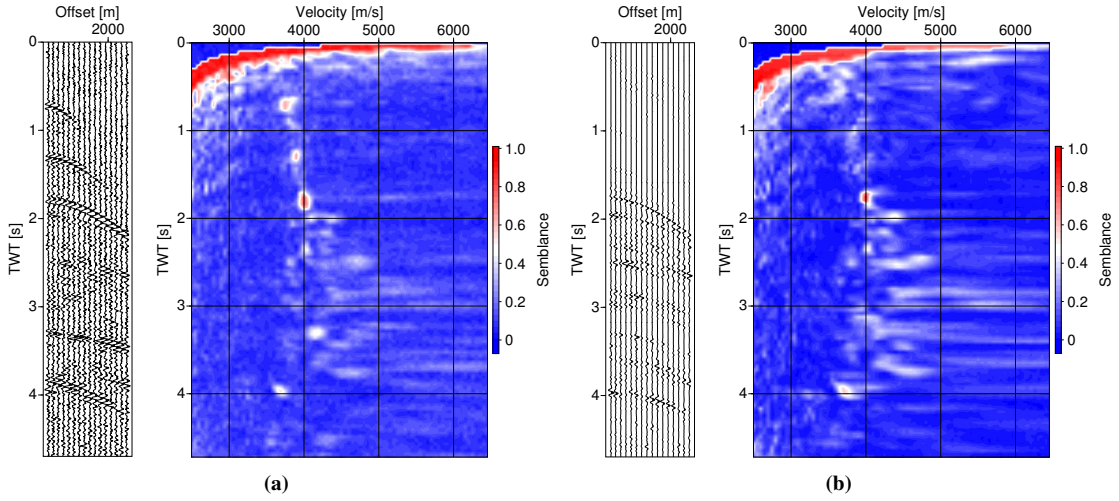

Figure 7: Results for a common-data-point (CDP) gather from x-line 300 and the corresponding velocity spectrum (a) before and (b) after prestack diffraction separation.

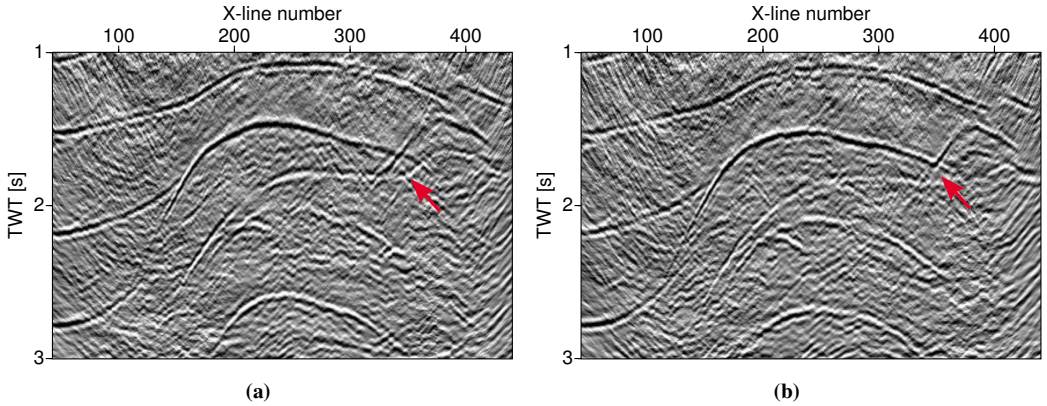

Figure 8: Results for in-line 130: prestack time migration using the velocity model obtained from data (a) before and (b) after prestack diffraction separation. Red arrows indicate events that were better focused using time migration velocities obtained from diffraction-only data.

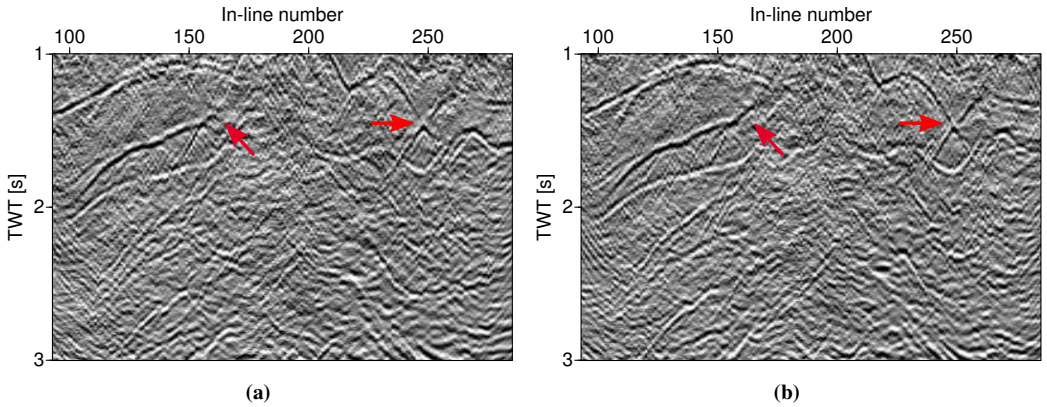

Figure 9: Results for x-line 300: prestack time migration using the velocity model obtained from data (a) before and (b) after prestack diffraction separation. Red arrows indicate events that were better focused using time migration velocities obtained from diffraction-only data.

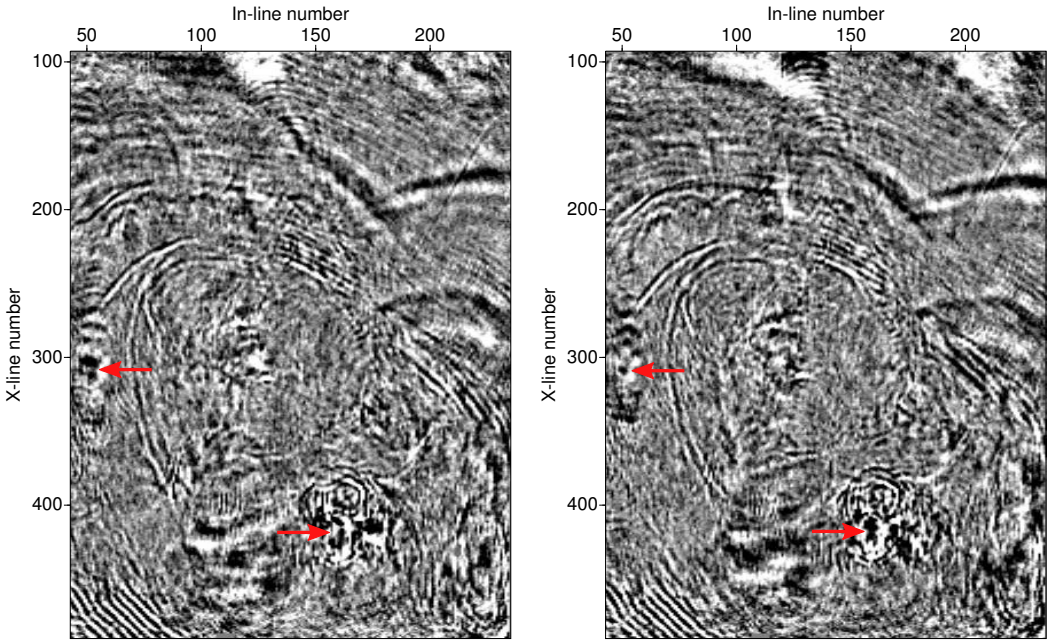

Figure 10: Results for time slice at 2.5 s: prestack time migration using the velocity model obtained from data (a) before and (b) after prestack diffraction separation. Red arrows indicate events that were better focused using time migration velocities obtained from diffraction-only data.

Hubral, P. (1983). Computing true amplitude reflections in a laterally inhomogeneous earth. *Geophysics*, 48:1051–1062.

Khaidukov, V., Landa, E., and Moser, T. J. (2004). Diffraction imaging by focusing-defocusing: An outlook on seismic superresolution. *Geophysics*, 69:1478–1490.

Mann, J. (2002). *Extensions and Applications of the Common-Reflection-Surface Stack Method*. PhD thesis, University of Karlsruhe.

Moser, T. J. and Howard, C. B. (2008). Diffraction imaging in depth. *Geophysical Prospecting*, 56:627–641.

Müller, N.-A. (2003). The 3D Common-Reflection-Surface stack – theory and application. Diploma thesis, University of Karlsruhe.

Robein, E. (2003). *Velocities, Time imaging, Depth imaging in Reflection seismics: Principles and Methods*. EAGE Publication, Houten.

Schleicher, J., Tygel, M., and Hubral, P. (1993). Parabolic and hyperbolic paraxial two-point traveltimes in 3D media. *Geophysical Prospecting*, 41:495–513.

Taner, M. and Koehler, F. (1969). Velocity spectra – digital computer derivation and applications of velocity functions. *Geophysics*, 34:859–881.